Electrode Shape and Collector Plate Spacing Effects on ESP Performance

Niels Finderup Nielsen, Christian Andersson
(FLSmidth Airtech, Ramsingsvej 30 DK 2500 Valby, E-mail: nfn@flsairtech.com)

Abstract: ElectroStatic Precipitator (ESP) suppliers are today conducted to reduce installation cost and due to world-wide environmental emission requirements also to improve performance. Two important and critical factors when designing high performance ESP's are discharge electrode design and collector plate spacing. Simulation and experimental results obtained in a pilot precipitator are used to investigate fundamental effects of the electrode shape for different collector plate spacing (Results – Part 1 – Simulations) and to study more "aggressive" electrodes for 300 mm and 500 mm plate spacing (Results – Part 2 – Experimental study). The ESP simulation model demonstrates, for different electrode shapes and collector plate spacing, basic characteristics of current-voltage-characteristics, current density at collecting plate, efficiency, turbulence level, strength of ionic wind, and effect of dust load. The experimental study focuses on electrode evaluation based on electrode shape and emitter orientation. An intensive study of several different electrode shapes has been carried out. ESP efficiency for wide spacing between collector plates is discussed in view of electrode shape and emitter orientation.

Keywords: Electrode shape, collector plate spacing, ESP simulation model, pilot ESP

1 INTRODUCTION

Low emission in general requires proper electrode design. Any electrode has a body, giving rise to field shadowing, i.e. regions on the collecting plate with zero or very low current density, it has emitters, wire fibulas, small plates, or regular spikes. Emitter geometry and orientation and electrode distance determine the corona starting voltage and the region with high and low current densities. Hence, proper discharge electrode design is a critical factor in order to design high performance ESP's [1]. Also one way to reduce installation cost is to widening collector plate spacing from 300 or 400 mm to say 500 or 600 mm without enlarging the ESP casing. But the larger spacing between collecting plates increases the space charge and requires higher operational voltage and by that more durable and expensive T/R sets. Hence more durable and rigid electrodes are needed [2], [3]. Hence it is also a challenge to find the optimal electrode shape for wide spacing between collecting plates.

This paper discusses work from a simulation model (Part 1) and pilot scale experiments (Part 2). Simulation results include current-voltage characteristics (CVCs) for clean and dust loaded ESPs, current density distributions at the collector plates, and ESP efficiency as well as strength of ionic wind and turbulence intensity versus electrode shape and plate spacing. Further the discharge electrode shape is related to processes with low and high dust load. These results are obtained with the FLSmidth Airtech ESP simulation model which includes most of the physical processes present in an ESP, such as dust resistivity, particle charging and the full three-dimensional fields of space charge, electric field strength, velocity, turbulence and concentration of a number of particle sizes. Pilot scale experiments places focus on efficiency of 300 mm and 500 mm spacing between collecting plates and the optimal electrode for wide collector plate spacing is discussed in view of critical parameters as electrode shape, emitter orientation etc. The FLSmidth Airtech pilot ESP is a two-field-one-duct filter with all necessary state of the art instrumentation including dust feeding system, PIACS controllers for adjusting the current from the high voltage rectifiers, PIACS manager system for recording various signals as velocity, emission, PIACS current, PIACS voltage, total plate current, pressure, temperature, dew point etc.

2 PILOT ESP SETUP

The FLSmidth Airtech pilot ESP is a two-field-one-duct precipitator with a dust feeding system at the inlet transition piece, flat dust hoppers, and an outlet cone. The first field has a duct width of 300 mm and the second field a duct width of 500 mm. The length of each field is 1.8 m, the height 1.5 m, and the 2 times 6 collecting plates (300 mm length) of each field are plane. The dust used in the present study is lime dust, so-called 'Faxe Foderkalk' (lime for cattle food). Resistivity has been measured, and at laboratory temperature and moisture the level is limited, less than 10^9 Ohm·cm. The particle size distribution has been measured in the FLS laboratory using a HELOS laser diffractiometer and the d_{50} is about 5.3 µm. The distribution is not log-normal as the $d_{15.9}$ = 1.25 µm and the $d_{84.1}$ = 40.4 µm. The dust mass density is 2,700 kg/m³.

3 SIMULATION MODEL

In the present study the simulation model solves the three-dimensional electrical and turbulent flow field and concentration of a number of different particle classes. The most important interactions between the different fields are included in the model and sketched by the arrows in Fig. 1. The electrical force is the main mechanism in the precipitator process and the three-dimensional model of [4] is used to calculate the electrical conditions influenced by ionic and

particle space charge. This model solves simultaneously the coupled electric and current density fields. The electric field takes into account the influence of ionic convection and diffusion due to corona discharge, the presence of particle space charge (electric field distortion) and the effect of dust resistivity at the collector plates. The weak interaction from the flow field on the electric field, i.e. the current due to convection of charge, is not included. However, the strong interaction of the electrical field (body force) on the flow field as well as the actual geometry is taken into account as seen from the induced secondary flows. The weak interaction from the particle field on the flow field is not included. The turbulent particle transport controlled by both electric field (including particle charging) and flow field (fluid particle dynamics) is modelled by an Eulerian approach due to the highly coupled problem, i.e. by treating particles as a second continuum phase characterized by its concentration, which also reduces the computational effort.

The three-dimensional electrostatic field between discharge electrode and collector plate in terms of potential and charge density is computed by solving

$$\nabla\cdot\boldsymbol{E} = (\rho_i+\rho_p)/\varepsilon_0\ , \quad \nabla\cdot\boldsymbol{J} = 0 \qquad (1)$$

$$\boldsymbol{J} = (\rho_i b_i \boldsymbol{E} - D_i\nabla\rho_i) + (\rho_p b_p \boldsymbol{E} - D_p\nabla\rho_p)$$

where: $\boldsymbol{E}= -\nabla\varphi$ is the electric field, φ the electric potential, ρ_i and ρ_p the space charge density of gas ions and particles, respectively, ε_0 the electric permittivity, $\boldsymbol{J}$ the current density, b_i and b_p the mobility of gas ions and particles, respectively, and D_i and D_p ion and particle diffusivity coefficients, respectively. For a detailed description of the FLSmidth Airtech simulation model including modelling procedure, coefficient values, geometry, computational mesh, and boundary conditions is referred to previous papers [4], [5], [6], [7], [8], [9].

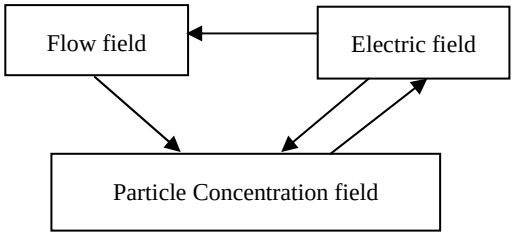

Fig. 1 Interaction between different fields of the ESP simulation model

4 EXPERIMENTAL SETUP

The FLSmidth Airtech pilot ESP is shown in Fig. 2. The air is sucked in through Viledon filter mats fitted to the inlet box. The flow rate generated by the fans running at constant rpm is controlled by a damper in the outlet duct controlled by an electromotor. The volume flow rate signal is the static pressure difference across the outlet cone, having been calibrated against a pitot-static tube.

As mentioned above the first field of the pilot ESP has a duct width of 300 mm and the second field a duct width of 500 mm. The length of each field is 1.8 m and the height 1.5 m. Having such small fields with a nominal height of 1.5 m, proper baffeling is of great importance in order to avoid sneakage above and below the electrode system. The top of the sections has been closed by horizontal covers of Teflon and the bottom with vertical baffles of Teflon. Likewise, baffles are inserted between plate curtains and compartment walls.

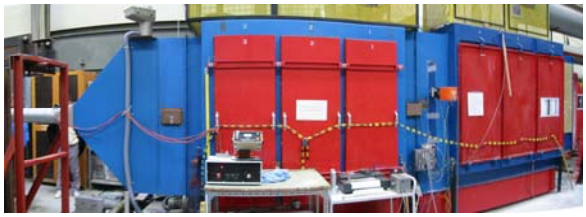

Fig. 2 FLSmidth Airtech pilot ESP

The current from the high voltage rectifiers is fed to each field via trunking and PIACS controllers, type II, control the current settings. HV capacitors ensure an almost pure DC. Collector plates are isolated and connected to ground via resistances making it possible to measure the current flowing to each plate-pair (opposite strips are connected in parallel). The plates are guided at the lower edge by a rapper bar insulated from the plates by Acetal plastic. A hand operated hammer is fitted outside, and rapping is done between measurement series.

The opacity meter, a SICK RM4 transmissiometer, is sending its light beam from bottom to top of the outlet funnel and, by use of a reflector, back again. A plane 45° mirror is placed between the SICK monitor and the hole in the funnel bottom, and before any recording is started the mirror is cleaned. Air purging of mirror and reflector keeps the optics clean during measurements. The SICK signal has been calibrated by gravimetrical measurements.

5 RESULTS AND DISCUSSIONS

The results have been divided into two parts. Part 1 is simulation results considering different elements related to the basic understanding of ESP behaviour for different electrode shapes and collector plate spacing. Part 2 is experimental results focusing on the optimal electrode for wide collector plate spacing. The setup of the pilot ESP described above has been used for both Part 1 and 2 and relevant operational data are shown in Table 1. Note that the mean particle diameter is relatively small and that the resistivity is relatively low.

Table 1 Pilot ESP operational data

CASE	Pilot ESP	
Field No/plate spacing [mm]	1/300	2/500
Electrical conditions: Current density level [mA/m^2]	0.01-1.0	0.01-1.0
Flow conditions: Mean bulk velocity V_0 [m/s] Temperature [^{o}C] ESP pressure [bar]	 1.3 22 1.0	 1.3 22 1.0

Dust particle conditions:		
Particle mean diameter [μm]	5.3	5.3
Particle std. deviation [μm]	not log nor.	not log nor
Number of particle classes	27	27
Particle mass density [kg/m^3]	2700	2700
Dust load [g/m^3]	1.0	1.0
Particle resistivity [Ω·cm]	10^9	10^9

5.1 Part 1 – Simulation Results

The simulations are carried out for field 1 only since it focuses on basic understanding and due to the fact that the simulation model is not restricted to 300 mm collector plate spacing. Three basic types of electrodes, Type-A, Type-B, and Type-C have been studied (Table 2). For Type-A and Type-B the emitters are pointing in the axial flow direction (0^o). For Type-C the emitters are pointing towards the collecting plate (90^o).

Table 2 Three type of electrodes used for model simulations. d denotes half duct width

Electrode Type	pin length [mm]	pin dist. from plate [mm]	pin spacing along electrode [mm] and orientation
Type-A	medium	d-0	100 , 0^o (round)
Type-B	large	d-0	100 , 0^o (round)
Type-C	large	d-17	100 , 90^o (sharp)

Focus has been placed on seven different kinds of results:

- Experimental verification;
- CVCs versus plate spacing and electrode shape;
- Current density distribution at collector plates;
- Efficiency versus corona power;
- Turbulence intensity versus plate spacing;
- Strength of ionic wind versus plate spacing;
- Effect of dust load.

These items are presented separately below.

Regarding turbulence intensity and strength of ionic wind these parameters are defined as follows. The turbulence intensity $\langle Tu\rangle_{yz} = (2\langle k\rangle_{yz}/3)^{1/2}/U_0$ calculated from turbulent kinetic energy $k_{yz} = ½ \langle \overline{u_k u_k} \rangle_{yz}$, and the bulk velocity $U_0 = \langle U\rangle_{yz}$ .The strength of ionic wind is represented by the mean value of magnitude of the velocity vector $\langle (V,W)\rangle_{yz}$. Hence these two parameters are average values over the cross section at a given axial position.

Experimental verification

Fig. 3 shows measured and computed current-voltage characteristics (CVCs) for a clean ESP with Type-A electrodes and collector plate spacing of 300 and 500 mm.

It is noted that the corona start potential is an input parameter for the computational model. This parameter has been fitted to the experimental data. For dust loaded gases other parameters of influence for CVCs are particle mass density, gas temperature, and pressure. These parameters are well controlled in a laboratory study but not always accessible for full scale studies. Anyway the computed CVCs for clean gases fits well with experimental values especially in the current density range of interest say 0.1 to 0.6 mA/m^2. The predicted corona start potential for the different spacing between collector plates and electrode types will be used in the present study for the dust loaded ESPs.

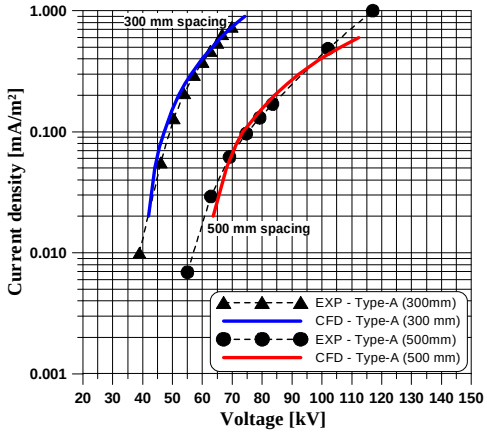

Fig. 3 Measured (symbols) and computed (solid coloured lines) CVCs for different Type-A electrode with 300 and 500 mm spacing between collecting plates. Clean pilot ESP setup

CVCs versus plate spacing and electrode shape

Calculated CVC's for the Type-A, Type-B and Type-C electrodes are shown in Fig. 4.

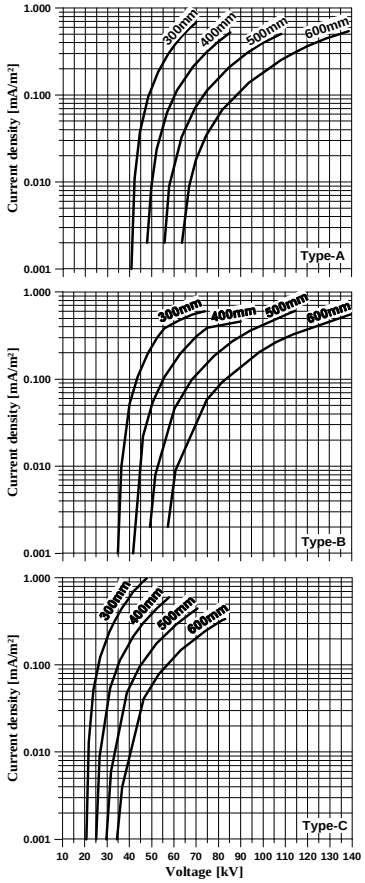

Fig. 4 Computed CVCs for Type-A, Type-B, and Type-C electrodes of the pilot ESP

Note the fairly high corona onset voltage of the Type-A and Type-B electrodes (round emitters) and the low corona onset voltage of the Type-C electrode (sharp emitter). For all electrodes we also notice higher corona onset voltage for larger plate spacing. As expected the narrower spacing between collecting plates the higher the current density at the same operational voltage. Hence, the narrower spacing between discharge electrode and collector plate leads to the strong electric field near the corona wire and by that corona current is easily generated.

Current density distribution at collector plates

The plot of Fig. 5(a) shows the current density distribution on the collecting surface for Type-A, Type-B, and Type-C electrodes at mean current density of 0.30 mA/m².

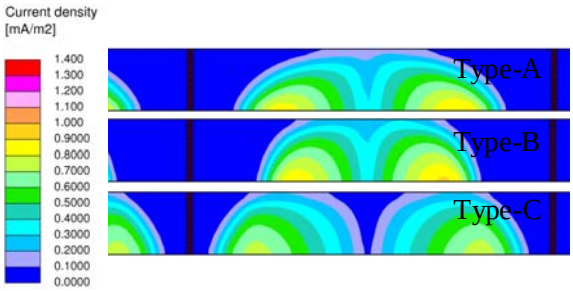

Fig. 5(a) Current density distribution on plates between first and second electrode for Type-A, Type-B, and Type-C electrodes at 300 mm spacing and mean current density of 0.3 mA/m^2. Vertical black line is electrode body and lower boundary is emitter centre line

For comparison Fig. 5(b) shows the current density distribution for Type-A electrode at collector plate spacing of 300 mm, 400 mm, 500 mm and 600 mm and at mean current density of 0.30 mA/m².

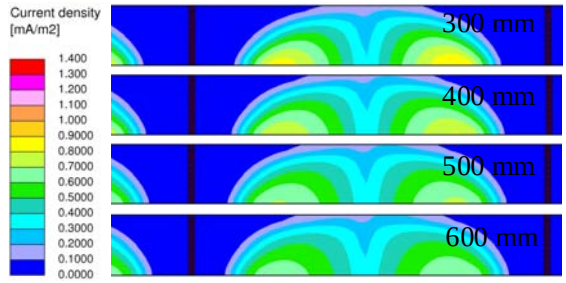

Fig.5(b) Current density distribution on the plate for Type-A electrode at 300 nm, 400 nm, 500 nm and 600 mm spacing at mean current density of 0.3 mA/m^2. Vertical black line is electrode body and lower boundary is emitter centre line

Type-A and Type-C electrodes have almost identical areas with low current density (below 0.1 mA/m^2) while Type-B electrode has a larger area with low current density (Fig. 5(a)). Further, as expected, clearly peak current density is decreasing for increasing spacing between collecting plates (Fig. 5(b)).

Efficiency versus corona power

Fig. 6(a) shows the efficiency for Type-A, Type-B, and Type-C electrodes at collector plate spacing of 300 mm, 400 mm, 500 mm and 600 mm.

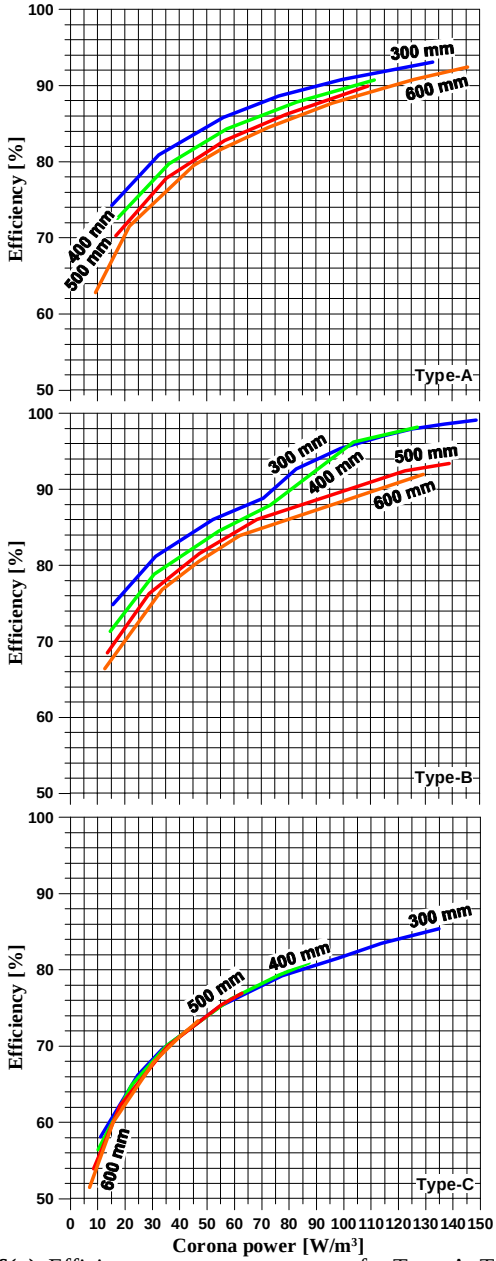

Fig. 6(a) Efficiency versus corona power for Type-A, Type-B, and Type-C electrodes at plate spacing of 300 nm, 400 nm, 500 nm and 600 mm

As expected ESP collection efficiency increases with increasing corona power. It can also be seen that the efficiency slightly decreases for increasing spacing between the collector plates for Type-A and Type-B electrodes while for Type-C electrode the efficiency is independent of plate spacing.

Fig. 6(b) shows the efficiency for the 3 different electrodes on the same plot but only for collector plate spacing of 300 nm and 600 mm. The present investigation indicates that Type-B electrode is the optimal electrode for 300 mm spacing between the collecting plates. Note however

that there is some scatter on the curve for high corona power. For 600 mm spacing Type-A and Type-B are equally good. Type-C electrode has the lowest efficiency for all collector plate spacing.

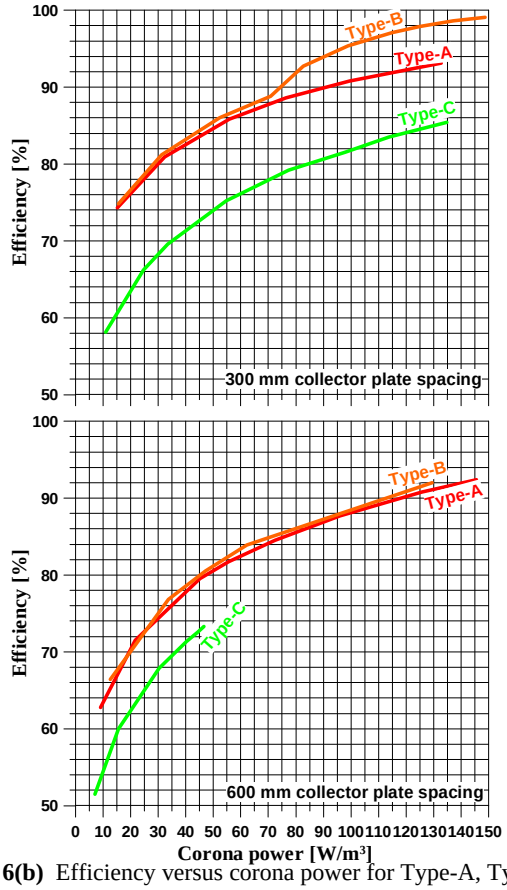

Fig. 6(b) Efficiency versus corona power for Type-A, Type-B, and Type-C electrodes at collector plate spacing of 300 nm and 600 mm

Turbulence intensity versus plate spacing

Calculated values of turbulence intensity (see definition above) are shown in Fig. 7 for Type-A, Type-B, and Type-C electrodes. All data on Fig. 7 are at identical mean current density of J_m = 0.3 mA/m^2 but note that the efficiency for Type-A, Type-B, and Type-C are η = 84%, η = 71%, and η = 70%, respectively. In general the turbulence intensity is almost identical for the different type of electrodes and further independent of spacing between collector plates.

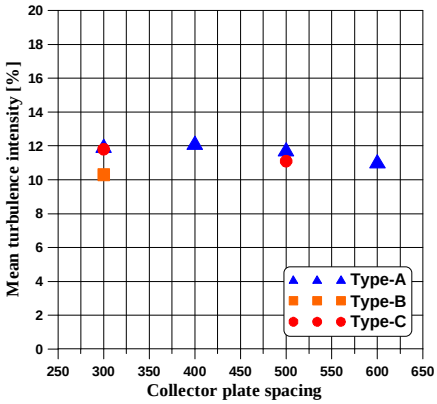

Fig. 7 Mean turbulence intensity versus collector plate spacing for Type-A, Type-B, and Type-C electrodes

Strength of ionic wind versus plate spacing

Fig. 8 shows the mean strength of ionic wind (see definition above) for Type-A, Type-B, and Type-C electrodes.

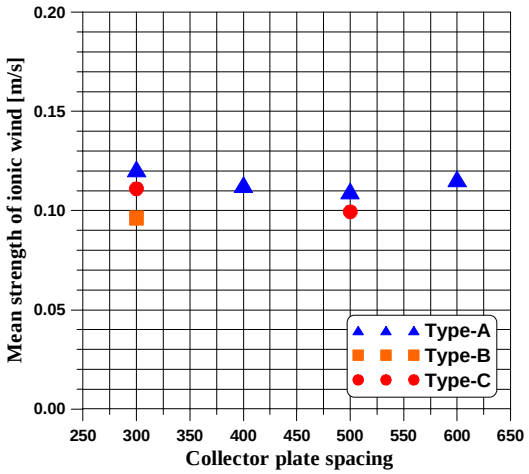

Fig. 8 Mean strength of ionic wind versus collector plate spacing for Type-A, Type-B, and Type-C electrodes

Identical trends as for the mean turbulence intensity are observed. The mean strength of ionic wind is almost identical for the different type of electrodes and further independent of spacing between collector plates. However calculations have shown that the staggered emitter arrangement, compared to the present non-staggered, has much lower mean strength of ionic wind but almost the same level of mean turbulence intensity.

Effect of dust load

In general there is a large difference between low and high dust load. For low load, say 1 g/m^3, the particle space charge is fairly low requiring moderate operational voltage for a given mean current density while for high dust load, say 10 g/m^3, the particle space charge is high requiring high operational voltage for a given mean current density. Fig. 9 shows CVC's for low and high dust load and plate spacing of 300 nm and 500 mm in both cases. In this case only Type-A electrode has been used.

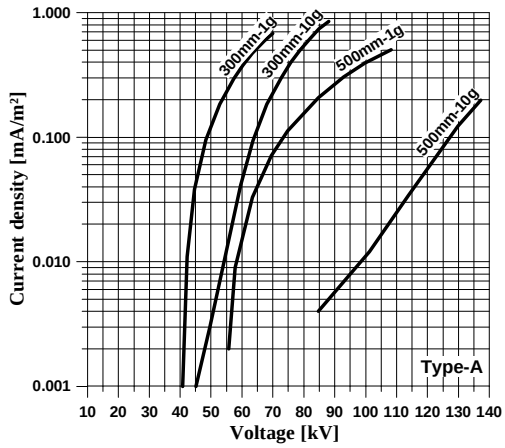

Fig. 9 CVC's for low (1g/m^3) and high (10g/m^3) dust load and 300 nm and 500 mm collector plate spacing. Type-A electrode

As expected higher dust load (or larger plate spacing) requires higher operational voltage for a given mean current density. Investigating the efficiency versus corona power for high dust load we obtain e.g. for 300 mm plate spacing efficiency η = 94.4% and corona power P=72.6 W/m^3 and for 500 mm plate spacing efficiency η = 95.3% for corona power P=86.0 W/m^3 both at equal mean current density of 0.3 mA/m^2 but at operational voltage of 72.6 kV and 144.8 kV for 300 nm and 500 mm spacing, respectively.

For low dust load the mean current density at each collector plate is identical downstream the ESP. But for high dust load the mean current density at the first collector plate is low due to high particle space charge and opposite on the last plate where the mean current density is high due to lower particle space charge. Fig. 10 shows the current density distribution between first and second electrode for low and high load (upper and middle figures) as well as one full field at high load (lower figure). Clearly, as expected, the mean distribution on each plate changes downstream the ESP.

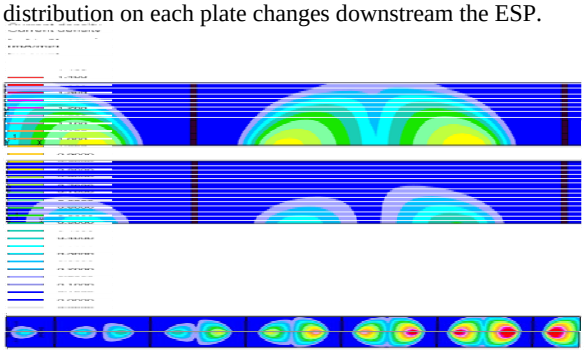

Fig. 10 Current density distribution on collector plate between first and second electrode for low and high dust load (upper and middle figures) and downstream field 1 for high dust load (lower figure). Mean current density is 0.3 mA/m^2 in both cases. Type-A electrode

Figs. 11 and 12 show the current density (Fig. 11) and particle space charge (Fig. 12) versus ESP length for low and high dust load.

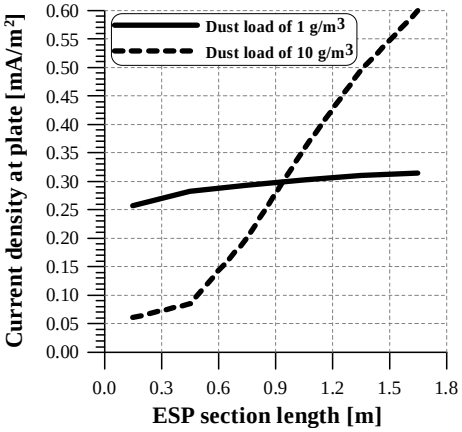

Fig. 11 Current density on plate downstream field 1 at low and high dust load. Mean current density is 0.3 mA/m^2. Type-A electrode

Clearly, for high dust load, the current density increases and the particle space charge decreases downstream the ESP clearly indicating trends discussed above.

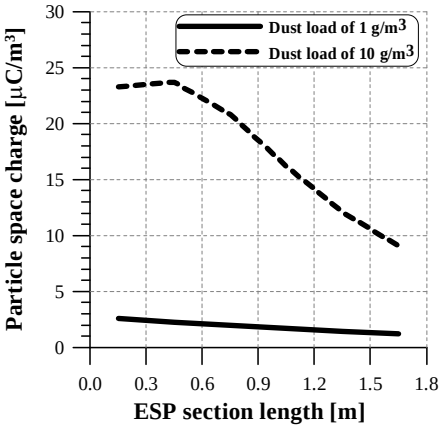

Fig. 12 Particle space charge downstream field 1 at low and high dust load. Mean current density is 0.3 mA/m^2 Type-A electrode

5.2 Part 2 – Experimental Results

The simulation results above indicates the need for investigating more "aggressive" type of electrodes with sharp emitters which could be useful for wide spacing between collecting plates. It turned out that the simulation model became unstable for some very aggressive electrodes with emitters pointing towards the collecting plate. Hence the pilot ESP is used for this study. 300 mm (field 1) and 500 mm (field 2) spacing between collecting plates have been studied. For both plate spacing seven different types of electrodes, including Type-A and Type-C from the simulation study, have been investigated (Table 3). Hence we have five new electrodes. For Type-A, Type-D the emitters are pointing in the axial flow direction (0^o). For Type-C, Type-E, Type-F, Type-G, and Type-H the emitters are pointing towards the collecting plate (90^o). Also note the different distances to the collecting plate for the different electrodes given in Table 3.

Table 3 Seven type of electrodes used for experimental investigation in pilot ESP. d denotes half duct width

Electrode Type	pin length [mm]	pin dist. from plate [mm]	pin spacing along electrode [mm] and orientation
Type-A	medium	d-0	100 , 0^o (round)
Type-C	large	d-17	100 , 90^o (sharp)
Type-D	short	d-0	76 , 0^o (sharp)
Type-E	short	d-13	76 , 90^o (sharp)
Type-F	large	d-43	100 , 90^o (sharp)
Type-G	medium	d-25	110 , 90^o (sharp)
Type-H	medium	d-29	110 , 90^o (sharp)

Efficiency

Fig. 13 shows the emission results from all seven electrodes presented here as penetration versus specifik work. Penetration is defined as emission based on the opacity meter reading divided by the inlet loading.

The results are shown for 300 mm collector plate spacing (results from field 1) and for 500 mm spacing (results from field 2) and both at 1.3 m/s mean bulk velocity (see Table 1 for other operational data).

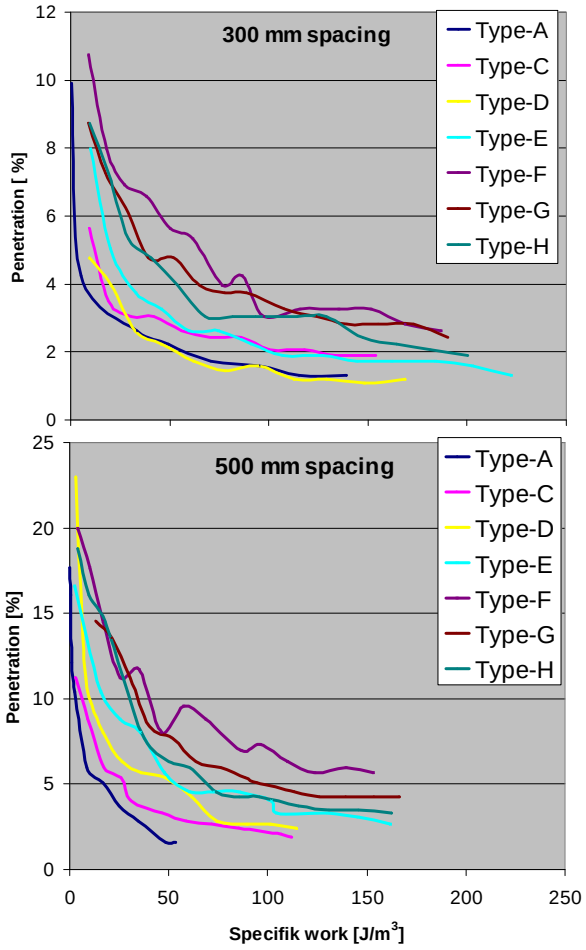

Fig.13 Penetration versus specific work for seven different electrodes (Table 3) at plate spacing of 300 (upper) and 500 mm (lower)

For 300 mm spacing Type-D is the better electrode however closely followed by Type-A. Comparing Type-D (emitters in flow direction) with Type-E (same as Type-D but emitter towards collecting plate) clearly Type-D is the better electrode. For 500 mm spacing it is evident that the blunt Type-A electrode as a whole gives the lowest penetration, most likely because the electric field at the plate surface is the highest. The more aggressive the electrode is, the higher the penetration.

Electrode evaluation

If we look more closely at the results at include both emission (penetration) and migration velocity an evaluation of the electrodes ends up with Table 4 for 300 mm spacing and Table 5 for 500 mm spacing. This investigation indicates that for 300 mm spacing Type-D (aggressive electrode with emitters in flow direction) is the better electrode and for 500 mm spacing Type-A (blunt electrode with emitters in the flow direction) is the better electrode. The electrodes fall in three main groups. The first is the best and is little aggressive for 300 mm spacing and blunt for 500 mm spacing requiring high operation voltage. The middle group is middle aggressive electrodes, and the last group contains the most aggressive electrodes.

Table 4 Electrode evaluation for 300 mm spacing between collector plates

Type-D	Type-A	Type-E	Type-C	Type-F	Type-G	Type-H
Best	Acceptable			Worst		

Table 5 Electrode evaluation for 500 mm spacing between collector plates

Type-A	Type-C	Type-D	Type-E	Type-H	Type-G	Type-F
Best	Acceptable			Worst		

6 CONCLUSIONS

In conclusion the present paper has shown the capabilities of both the FLSmidth Airtech ESP simulation model and the pilot ESP. The simulation model has demonstrated that it can predict parameters that is difficult to measure even in a laboratory pilot model setup. The simulation results, investigating three different electrodes Type-A, Type-B, and Type-C shows, as expected, that the narrower spacing between collecting plates the higher the current density at the same operational voltage. No clear corelation between ESP efficiency and current density distribution at the collecting plates for the different electrodes was found. However, it should be noted that attempts to differentiate between the different electrodes only has a meaning if the dust load is high as illustrated in the present study. At low dust load the mean current density at each collector plate is at a constant level downstream the ESP. Further it was demonstrated that the most efficient electrode shape for both 300 mm and 600 mm spacing was a “long” electrode with round emitters (blunt electrode type) pointing in the flow direction (Type-B electrode). Also, the simulations indicates that both the turbulence intensity and the strength of ionic wind seems to be almost identical for the different type of electrodes and further independent of spacing between collector plates. Finally the simulation model demonstrated that high dust load, or larger plate spacing, requires high operational voltage for a given mean current density, as expected, and that for high dust load the mean current density at the first collector plate is low due to high particle space

charge and opposite on the last plate where the mean current density is high due to lower particle space charge. The experimental results investigating several different electrodes clearly demonstrated that the most efficient electrode is one with the emitters pointing in the flow direction. Futrher it seems that a sharp emitter tip (Type-D; short little aggressive electrode type) is slightly more efficient for 300 mm plate spacing but that a round emitter tip (Type-A; medium long blunt electrode type) is clearly more efficient for 500 mm plate spacing. Note that the electrode shape of Type-A and Type-B of the simulation study is similar but with different emitter length. Anyway the experimental study clearly shows that aggressive electrodes are not preferable for wide spacing between collecing plates and in any case high operational voltage is required resulting in expensive T/R sets. However further analysis is required in order to obtain a final conclusion.

REFERENCES

1. Jaworek, A, Krupa, A & Czech, T., Modern electrostatic devices and methods for exhaust gas cleaning: A brief review, J. Electrostatics, 65 (2007), 133-155.
2. Darby, K., Plate spacing effect on precipitator performance. Proceedings of second International Conference on Electrostatic Precipitation, November 1984, Kyoto, Japan, 376-383.
3. Kim, Y.J., Jeong, S.H., Hong, W.S.Cho, S.S. and Ham, B.H., Effect of the plate spacing and disharge electrode shape on the efficiency of wide plate spacing electrostatic precipitator. Proceedings of Seventh International Conference on Electrostatic Precipitation, September 20-25, 1998, Kyongju, Korea, 590-595.
4. Zamany, J., 1992, Modelling of particle transport in Commercial Electrostatic Precipitators, Ph.D Thesis, ATV EF 316, Technical University of Denmark and FLS Airtech A/S (formerly FLS miljø a/s).
5. Zamany, J., 1995a, Numerical modeling of electrodynamic conditions influenced by particle space charge and resistivity in electrostatic precipitators of complex geometry for industrial applications, Inst Phys Conf Ser No 143: 357-362.
6. Zamany, J., 1995b, Numerical modeling of electrodynamic conditions influenced by particle space charge and resistivity in electrostatic precipitators of complex geometry for industrial applications, FLS Airtech A/S (formerly FLS miljø) Internal report, FLS Airtech, Valby, Denmark.
7. Akoh, E. & Nielsen, N.F., 2000, EFP-2000: Electrostatic Precipitation–Reduction of Emission and Energy Consumption, Software Specification, FORCE Technology (formerly DMI) report: TN.2000878, FORCE Technology, Lyngby, Denmark.
8. Lind, L., Nielsen, N.F., Larsen, P.S., Hove, E.A., 2004, Simulation of particle transport in electrostatic precipitators, Proceedings of 9th. International Conference on Electrostatic Precipitation, May. 17-21, 2004, Mpumalanga, South Africa, Paper A24.
9. Nielsen, N.F., Larsen, P.S., Löfström, C, 2006, Secondary flows and turbulence for staggered and non-staggered electrode emitters. Proceedings of 10th. International Conference on Electrostatic Precipitation, June. 25-29, 2006, Cairns, Australia, Paper 2A3.